DOI: 10.1002/chem.201000923

Do Trinuclear Triplesalen Complexes Exhibit Cooperative Effects? Synthesis, Characterization, and Enantioselective Catalytic Sulfoxidation by Chiral Trinuclear Fe^{III} Triplesalen Complexes

Chandan Mukherjee, Anja Stammler, Hartmut Bögge, and Thorsten Glaser*[a]

Abstract: The chiral triplesalen ligand H_6chand provides three chiral salen ligand compartments in a *meta*-phenylene arrangement by a phloroglucinol backbone. The two diastereomeric versions H_6chand^{RR} and H_6chand^{rac} have been used to synthesize the enantiomerically pure chiral complex [$(FeCl)_3$(chand^{RR})] (**3^{RR}**) and the racemic complex [$(FeCl)_3$(chand^{rac})] (**3^{rac}**). The molecular structure of the free ligand H_6chand^{rac} exhibits at the terminal donor sides the O-protonated phenol–imine tautomer and at the central donor sides the N-protonated keto–enamine tautomer. The trinuclear complexes are comprised of five-coordinate square-pyramidal Fe^{III} ions with a chloride at the axial positions. The crystal structure of **3^{rac}** exhibits collinear chiral channels of ~11 Å in diameter making up 33.6% of the volume of the crystals, whereas the crystal structure of **3^{RR}** exhibits voids of 560 Å^3. Mössbauer spectroscopy demonstrates the presence of Fe^{III} high-spin ions. UV/Vis spectroscopy is in accordance with a large delocalized system in the central backbone evidenced by strong low-energy shifts of the imine π–π* transitions relative to that of the terminal units. Magnetic measurements reveal weak intramolecular exchange interactions but strong magnetic anisotropies of the Fe^{III} ions. Complexes **3^{rac}** and **3^{RR}** are good catalysts for the sulfoxidation of sulfides providing very good yields and high selectivities with **3^{RR}** being enantioselective. A comparison of **3^{RR}** and [FeCl(salen′)] provides higher yields and selectivities but lower enantiomeric excess values (*ee* values) for **3^{RR}** relative to [FeCl(salen′)]. The low *ee* values of **3^{RR}** appeared to be connected to a strong ligand folding in **3^{RR}**, opening access to the catalytically active high-valent Fe–O species. The higher selectivity is assigned to a cooperative stabilization of the catalytically active high-valent Fe–O species through the phloroglucinol backbone in the trinuclear complexes.

Keywords: homogeneous catalysis · iron · magnetic properties · N,O ligands · stereoselective catalysis

Introduction

The synthesis of enantiomerically pure sulfoxides by the oxidation of prochiral sulfides has drawn considerable attention in the last decade.[1] Enantiomerically pure sulfoxides have been used as both building blocks and versatile chiral controllers for the synthesis of natural products and biologically active compounds.[1–5] Several methods for the synthesis of enantiopure sulfoxides were described,[6–19] including Andersen's method,[6] in which Grignard reagents have been used with chiral sulfinates. The direct asymmetric oxidation of prochiral sulfides catalyzed by enzymes or chiral metal complexes is of interest due to their simplicity, low toxicity, and economical benignity.

Enantioselective oxidation of prochiral sulfides to sulfoxides with chiral complexes of titanium,[10,11,20–22] vanadium,[15,23,24] and manganese[7,12,25,26] as catalysts has been extensively investigated. In contrast, chiral iron complexes are less studied as asymmetric catalysts for this reaction. In 2003, the asymmetric sulfoxidation of prochiral sulfides with H_2O_2 as an external oxidant was reported by an in situ reaction using [$Fe(acac)_3$] (acac = acetylacetonate) and a chiral ligand as the catalyst.[27] The catalytic properties of the nonchiral parent iron salen complex for sulfoxidation were reported in 2002.[28] Application of the chiral salen derivative, that is, by using the Jacobsen ligand H_2salen′,[29] showed that the chiral iron complex catalyzes the asymmetric oxidative formation of sulfoxides from prochiral sulfides in the presence of the external oxidant PhIO.[30]

[a] C. Mukherjee, A. Stammler, H. Bögge, T. Glaser
Lehrstuhl für Anorganische Chemie I
Fakultät für Chemie, Universität Bielefeld
Universitätsstr. 25, 33615 Bielefeld (Germany)
Fax: (+49) 521-106-6003
E-mail: thorsten.glaser@uniso-bielefeld.de

Supporting information for this article is available on the WWW under http://dx.doi.org/10.1002/chem.201000923.

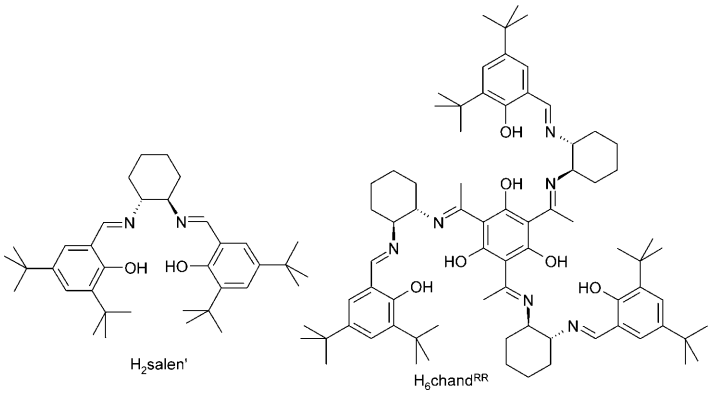

In our ongoing efforts[31–47] for a rational synthesis of new single-molecule magnets (SMMs) and asymmetric oxidation catalysts, we have developed the chiral triplesalen ligand H_6chand in the all *R*,*R* form, H_6chand^{RR}, and in the all *S*,*S* form, H_6chand^{SS},[44] which we envision as the C_3-symmetric trinuclear extension of the Jacobsen ligand H_2salen′.[29] The three chiral subunits of the ligand H_6chand are connected with each other via a phloroglucinol (1,3,5-trihydroxybenzene) bridging unit. Hence, obeying the spin-polarization mechanism,[48–52] ferromagnetic interactions between the three metal salen units may lead to high-spin ground states.[53–62] Trinuclear Cu^{II} triplesalen complexes indeed show a high-spin ground state with ferromagnetic coupling between three Cu^{II} centers.[35,39] Besides that, we have been able to synthesize several heptanuclear complexes $M_6M'^{n+}$ with $M_3M'M_3$ topology by using two trinuclear triplesalen complexes as molecular building blocks and hexacyanometallate as the bridging unit.[37,42,47] Among them, $[\{Mn^{III}{}_3(talen'^{Bu_2})\}_2\{Cr^{III}(CN)_6\}](BPh_4)_3$ (H_6talen = 2,4,6-tris{1-[2-(3,5-di-*tert*-butylsalicylaldimino)-2-methylpropylimino]ethyl}-1,3,5-trihydroxybenzene) behaves as a SMM.[37]

Trinuclear triplesalen complexes exhibit bowl-shaped molecular structures.[35,39] Hence, we thought trinuclear triplesalen complexes of the chiral ligand H_6chand would likely provide a chiral pocket that should be ideally suited for asymmetric catalysis. Furthermore, a mechanism was established for the asymmetric nucleophilic ring opening of epoxides by chromium salen complexes, involving catalytic activation of both the nucleophile and the electrophile in a bimetallic rate-determining step.[63–65] By using covalently linked dinuclear salen complexes, not only the intramolecular pathway but also an intermolecular pathway was enhanced. This observation "indicates that dimer reacts more rapidly with dimer, than does monomer with monomer and suggests that the design of covalently linked systems bearing three or more metal salen units may be worthwhile".[66]

Recently, we reported the successful synthesis and characterization of the chiral triplesalen ligands H_6chand^{RR} and H_6chand^{SS}, and their trinuclear Mn^{III} complexes in conjugation with their catalytic activity for the asymmetric epoxidation of unfunctionalized olefins.[44] Herein, we report the synthesis and characterization of the racemic form of the ligand H_6chand^{rac}, its racemic trinuclear Fe^{III} complex $[(FeCl)_3(chand^{rac})]$, and the chiral trinuclear Fe^{III} complex $[(FeCl)_3(chand^{RR})]$. The catalytic properties of the complexes for the sulfoxidation of sulfides, either asymmetric or not, in the presence of PhIO or NaOCl as external oxidants have been investigated. Furthermore, comparison of the catalytic efficiencies of the trinuclear $[(FeCl)_3(chand^{RR})]$ complex to the mononuclear [FeCl(salen′)] complex allows us to evaluate the presence of cooperative effects in the trinuclear complex.

Experimental Section

Materials: All reagents were obtained from commercial sources and used as supplied, unless otherwise noted. 2,4,6-Triacetyl-1,3,5-trihydroxybenzene (**1**) was prepared according to the reported procedure.[67] The synthesis of 2,4,6-tris{1-[(1*R*,2*R*)-2-aminocyclohexylimino]ethyl}-1,3,5-trihydroxybenzene (**2^{RR}**) and 2,4,6-tris{1-[(1*R*,2*R*)-2-(3,5-di-*tert*-butylsalicylaldimino)cyclohexylimino]ethyl}-1,3,5-trihydroxybenzene (H_6chand^{RR}) were reported previously.[44] Enantiomerically pure *trans*-(*R*,*R*)-1,2-cyclohexanediamine was obtained by an established kinetic resolution.[68] The purity of thioanisole, benzyl phenyl sulfide, 4-bromo thioanisole, and methyl *p*-tolyl sulfide was checked by ^{1}H NMR spectroscopy and gas chromatography (GC). Iodosylbenzene was prepared by the hydrolysis of iodobenzene diacetate and was kept in the dark with a coating of aluminum foil.

2,4,6-Tris[1-(2-aminocyclohexylimino)ethyl]-1,3,5-trihydroxybenzene (2^{rac}): 2,4,6-Triacetyl-1,3,5-trihydroxybenzene (**1**) (0.520 g, 2.063 mmol) was added to a solution of *trans*-(±)-1,2-cyclohexanediamine (1.425 g, 12.480 mmol) in EtOH (20 mL) and the resulting mixture was stirred at room temperature for 20 h during which time the color of the solution changed to deep red. The solution was filtered and evaporated under vacuum at 50 °C to yield a red oil. Et_2O (100 mL) was added to the red oil and the mixture was stirred for 1 h. The suspension was filtered to remove a light-yellow solid and the filtrate was evaporated under vacuum at 50 °C to yield again a red oil. This oil was dissolved in H_2O (30 mL) and extracted with CH_2Cl_2 (100 mL). The CH_2Cl_2 solution was further washed with water (2×25 mL) and dried over Na_2SO_4. Upon evaporation of CH_2Cl_2, a sticky yellow oil was obtained. Yield: 0.67 g (60 %); IR (KBr): $\tilde{\nu}$ = 3431 (m), 3370 (m), 3293 (m), 2930 (s), 2857 (s), 1533 (s), 1458 (m), 1449 (m), 1420 (m), 1373 (m), 1340 (m), 1321 (m), 1267 (w), 1244 (w), 866 (w), 845 (w), 820 cm^{-1} (w); ^{1}H NMR (500.05 MHz, $CDCl_3$): δ = 1.15–1.44 (m, 12H), 1.65–1.96 (m, 18H), 2.56–2.64 (3 s, 9H), 2.74–2.90 (m, 3H), 3.25–3.43 (m, 3H), 13.11–14.39, 18.53 ppm (br s, 3H); ^{13}C NMR (125.77 MHz, $CDCl_3$): δ = 18.5, 19.1, 19.5, 24.4, 24.5, 24.6, 24.7, 24.8, 30.4, 31.5, 32.3, 32.4, 32.7, 34.1, 34.2, 54.7, 54.8, 55.0, 60.0, 60.3, 60.8, 105.8, 170.1, 173.0, 183.5, 184.7, 185.6 ppm; MS-ESI (+ve, CH_2Cl_2): *m*/*z*: 541.4 $[M+H]^+$; elemental analysis calcd (%) for $C_{30}H_{48}N_6O_3 \cdot 1\,CH_2Cl_2 \cdot 0.5\,Et_2O$: C 59.80, H 8.36, N 12.68; found: C 60.00, H 8.11, N 12.77.

2,4,6-Tris{1-[2-(3,5-di-*tert*-butylsalicylaldimino)cyclohexylimino]ethyl}-1,3,5-trihydroxybenzene (H_6chand^{rac}): A solution of half-unit **2^{rac}** (0.546 g, 1.00 mmol) and 3,5-di-*tert*-butylsalicylaldehyde (0.710 g, 3.03 mmol) in MeOH (15 mL) was stirred for 20 h, during which time a yellow precipitate formed. This filtrate was isolated by filtration, washed with MeOH, and dried under air. Yield: 0.78 g (66 %); IR (KBr): $\tilde{\nu}$ = 3460 (w), 2951 (s), 2862 (m), 1628 (s), 1593 (m), 1539 (s), 1454 (s), 1441 (s), 1392 (m), 1362 (m), 1346 (m), 1273 (m), 1252 (m), 1242 (m), 1172 (m), 982 (w), 878 (w), 829 (w), 771 cm^{-1} (w); ^{1}H NMR (500.15 MHz, $CDCl_3$): δ = 1.12–1.29 (m, 27H), 1.45–2.15 (m, 51H), 2.46–2.66 (m, 9H), 3.18–3.35 (m, 3H), 3.69–3.94 (m, 3H), 6.95–7.06 (m, 3H), 7.35–7.38 (m, 3H), 8.31–8.50 (m, 3H), 13.35–15.40, 18.34–18.56 ppm (m, 3H); ^{13}C NMR (125.77 MHz, $CDCl_3$): δ = 18.4, 18.5, 18.9, 19.0, 19.2, 19.4, 23.6, 23.7, 24.1, 24.2, 24.3, 29.2, 29.3, 29.4, 30.4, 31.0, 31.2, 31.3, 31.7, 31.8, 32.1, 33.1, 33.2, 33.8, 33.9, 34.8, 34.8, 56.4, 57.0, 57.1, 57.3, 72.2, 72.3, 72.6, 72.7, 99,9, 105.4, 105.6,

105.7, 106.2, 117.3, 117.4, 117.5, 117.6, 117.7, 125.9, 126.0, 126.5, 126.8, 127.0, 127.1, 136.1, 136.2, 136.3, 136.4, 139.7, 139.8, 140.0, 157.6, 157.7, 157.8, 165.7, 166.5, 166.6, 166.7, 170.0, 170.1, 172.4, 172.4, 172.7, 172.9, 179.7, 183.3, 183.4, 184.2, 184.4, 185.0, 185.3, 185.6 ppm; MS-ESI (+ve, CH_2Cl_2): *m/z*: 1190.8 $[M+H]^+$; elemental analysis calcd (%) for $C_{75}H_{108}N_6O_6$: C 75.72, H 9.15, N 7.06; found: C 75.60, H 9.05, N 7.03.

$[(FeCl)_3(chand^{rac})]$ (3^{rac}): Anhydrous $FeCl_3$ (0.152 g, 0.94 mmol), the ligand H_6chand^{rac} (0.350 g, 0.294 mmol), and Et_3N (0.1 mL) were added to a solvent mixture of CH_3CN (25 mL) and MeOH (10 mL). The resulting deep-purple solution was heated at reflux for 15 min. Stirring for additional 15 h caused the deposition of a purple microcrystalline solid that was isolated by filtration, washed with CH_3CN, and recrystallized from CH_3CN/CH_2Cl_2. Yield: 0.212 g (50%); IR (KBr): $\tilde{\nu}$ = 2951 (s), 2866 (s), 1626 (s), 1537 (s), 1487 (s), 1435 (m), 1389 (m), 1348 (w), 1254 (s), 1238 (m), 1175 (w), 1049 (w), 822 (w), 598 (w), 544 cm^{-1} (w); MALDI-TOF-MS: *m/z*: 1457.0 $[M]^+$, 1421.9 $[M-Cl]^+$; elemental analysis calcd (%) for $C_{75}H_{102}Cl_3Fe_3N_6O_6 \cdot 1.5\,H_2O$: C 60.67, H 7.13, N 5.66; found: C 60.66, H 7.03, N 5.75.

$[(FeCl)_3(chand^{RR})]$ (3^{RR}): A solution of the ligand H_6chand^{RR} (0.800 g, 0.67 mmol) in CH_3CN (30 mL) was treated with anhydrous $FeCl_3$ (0.350 g, 2.16 mmol) and Et_3N (0.4 mL). The resulting deep-purple solution was heated at reflux for 15 min. Stirring for an additional 15 h at room temperature caused the deposition of a purple microcrystalline solid that was isolated by filtration, washed with CH_3CN, and recrystallized from $MeOH/CH_3CN/CH_2Cl_2$. Yield: 0.392 g (40%); IR (KBr): $\tilde{\nu}$ = 2952 (s), 2864 (m), 1626 (s), 1537 (s), 1479 (s), 1435 (s), 1389 (m), 1362 (m), 1348 (m), 1254 (s), 1209 (m), 1173 (m), 1049 (w), 822 (w), 598 (w), 542 cm^{-1} (w); MS-ESI (+ve, CH_2Cl_2): *m/z*: 1458.5 $[M+H]^+$, 1420.6 $[M-Cl]^+$; MALDI-TOF-MS: *m/z*: 1457.1 $[M]^+$, 1422.0 $[M-Cl]^+$, 1385.9 $[M-2Cl]^+$; $[\alpha]_D^{20}$ = −650.0 (±5.0) (*c* = 0.02 in $CHCl_3$); elemental analysis calcd (%) for $C_{75}H_{102}Cl_3Fe_3N_6O_6$: C 61.80, H 7.05, N 5.76; found: C 61.84, H 6.97, N 5.74.

General procedure for catalytic reactions: Complex **3** (7.30 mg, 0.005 mmol) was dissolved in CH_2Cl_2 (2 mL). The sulfide substrate (0.1 mmol) and iodosylbenzene (49.0 mg, 0. 223 mmol) were added to this solution and the mixture was stirred at room temperature for 15 h. The solvent was evaporated and the residue treated with CH_3CN (0.2 mL) and passed through a short SiO_2 column. The column was washed with CH_3CN (10 mL). The resulting solution was evaporated and ^1H NMR spectra were recorded after dissolving the residue in $CDCl_3$ (0.6 mL). The conversion was calculated from the area of the sulfide, sulfoxide, and sulfone signals obtained in the ^1H NMR spectrum by using the formula % conversion = 100 × ([product])/([substrate] + [product]). GC and GCMS measurements were also performed to identify the products.

X-ray crystallography: Yellow crystals of $H_6chand^{rac} \cdot 2\,CH_3CN \cdot MeOH$ were grown by slow evaporation of a $MeOH/CH_3CN/CH_2Cl_2$ solvent mixture. Dark-brown crystals of 3^{rac} were grown by slow evaporation of a CH_3CN/CH_2Cl_2 solvent mixture and black crystals of 3^{RR} by slow evaporation of a $MeOH/CH_3CN/CH_2Cl_2$ solvent mixture.

The single crystals were removed from the mother liquor, coated with paraffin oil and immediately cooled to 173(2) K on a Bruker AXS SMART diffractometer (three circle goniometer with 1 K CCD detector, $Mo_{k\alpha}$ radiation, graphite monochromator. Hemisphere data collection in ω at 0.3° scan width in three runs with 606, 435, and 230 frames (ϕ = 0, 88, and 180°; detector distance of 5 cm). An empirical absorption correction by using equivalent reflections was performed with the program SADABS 2.10.[69] The structures were solved with the program SHELXS-97[70] and refined by using SHELXL-97.[70]

As the crystals of $H_6chand^{rac} \cdot 2\,CH_3CN \cdot MeOH$ were very small, the structure could only be refined up to 2θ = 46. However, the O–H and N–H hydrogen atoms of H_6chand^{rac} could be located in a difference Fourier synthesis and freely be refined with $U(H) = 1.2\,U(O/N)$. The measured crystal of 3^{rac} turned out to be a racemic twin with a ratio of 0.67/0.33 for the two components. The unit cell of 3^{rac} contains a huge void of approximately 4900 Å^3. A refinement with a "squeezed"[71] data set, however, resulted in a nearly identical *R* value and positional and thermal parameters. Thus the original data set was retained. The unit cell of 3^{RR} contains two voids of approximately 560 Å^3. No solvent molecule could be located in these voids. Crystal data and further details concerning the crystal structure determination are summarized in Table 1.

Table 1. Crystallographic data for $H_6chand^{rac} \cdot 2\,CH_3CN \cdot MeOH$, 3^{rac}, and 3^{RR}.

Compound	$H_6chand^{rac} \cdot 2\,CH_3CN \cdot MeOH$	3^{rac}	3^{RR}
chem. Formula	$C_{75}H_{108}N_6O_6 \cdot 2CH_3CN \cdot MeOH$	$C_{75}H_{102}Cl_3Fe_3N_6O_6$	$C_{75}H_{102}Cl_3Fe_3N_6O_6$
F_w	1303.82	1457.53	1457.53
T [K]	173(2)	173(2)	173(2)
space group	$P2_1/n$	$P6_1$	$P2_12_12_1$
a [Å]	16.2391(6)	30.1782(18)	15.2409(9)
b [Å]	19.4933(7)	–	20.6903(12)
c [Å]	25.6868(10)	18.9099(17)	26.4118(16)
β [°]	106.280(1)		
V [Å^3]	7805.2(5)	14914.4(18)	8328.7(9)
Z	4	6	4
ρ_{calcd} [g cm^{-3}]	1.110	0.974	1.162
λ [Å]; $\mu(Mo_{K\alpha})$ [mm^{-1}]	0.71073; 0.071	0.71073; 0.553	0.71073; 0.660
crystal size [mm]	0.40 × 0.14 × 0.12	0.30 × 0.20 × 0.10	0.50 × 0.40 × 0.30
coll. reflns; θ_{max}	33307; 23.00	67060; 24.00	42975; 24.99
unique reflns	10845 (R(int) = 0.0407)	15395 (R(int) = 0.2143)	14631 (R(int) = 0.0398)
obs. reflns ($I > 2\sigma(I)$)	6668	5519	12776
Parameters	870	805	859
GooF[a] on F^2	1.039	0.952	1.068
$R1$[b]; $wR2$[c] ($I > 2\sigma(I)$)	0.0758; 0.2027	0.0869; 0.1748	0.0442; 0.0916
abs. struct. parameter[d]		0.33(3)	0.010(11)
max/min residuals [e Å^{-3}]	0.853, −0.446	0.760, −0.251	0.427, −0.246

[a] $GooF = [\Sigma[w(F_o^2 - F_c^2)^2]/(n-p)]^{1/2}$. [b] $R1 = \Sigma||F_o| - |F_c||/\Sigma|F_o|$. [c] $wR2 = [\Sigma[w(F_o^2 - F_c^2)^2]/\Sigma[w(F_o^2)^2]]^{1/2}$, in which $w = 1/[\sigma^2(F_o^2) + (aP)^2 + bP]$, $P = (F_o^2 + 2F_c^2)/3$. [d] See reference [104].

CCDC-777337–777339 contain the supplementary crystallographic data for this paper. These data can be obtained free of charge from The Cambridge Crystallographic Data Centre via www.ccdc.cam.ac.uk/data_request/cif.

Other physical measurements: FTIR spectra were recorded on a Shimadzu 8300 spectrometer as KBr pellets. ^1H and ^{13}C NMR spectra were recorded on a Bruker DRX500 by using the solvent as an internal standard. ESI Mass spectra were obtained on a Bruker Esquire 3000 mass spectrometer. MALDI TOF mass spectra were recorded with a Voyager DE instrument. Elemental analyses were carried out in the Microanalysis Laboratory, Bielefeld University. GC analyses were performed on a Shimadzu GC2010 and GCMS analysis on a Shimadzu QP2010S. The enantiomeric excess (*ee*) values were determined by HPLC on a chiral stationary phase (Chiralcel OD-H, 254 nm, 20 °C, hexane/*i*PrOH 9:1 or 99:1 (4-bromo thioanisole), flow rate = 0.5 or 1.0 mL min^{-1} (4-bromo thioanisole).

Magnetic susceptibility data were measured from powder samples of solid material in the temperature range 2–290 K by using a SQUID magnetometer (Quantum Design MPMS XL-7 EC) with a field of 1.0 T. The

experimental data were corrected for underlying diamagnetism by the use of tabulated Pascal's constants.

^{57}Fe Mössbauer spectra were recorded on an alternating constant-acceleration spectrometer. The minimal line width was 0.24 mm s^{-1} full width at half height. The sample temperature was maintained constant in a bath cryostat (Wissel MBBC-HE0106). ^{57}Co/Rh was used as the radiation source. Isomer shifts were determined relative to α-iron at room temperature.

Results and Discussion

Synthesis and characterization: In contrast to the synthesis of symmetrical salen-type ligands by one-pot condensation reactions of one diamine with two identical aldehyde or ketone derivatives, synthesis of unsymmetrical salen-type ligands is more challenging[72] and requires a so-called half unit.[73–76] After several optimization steps, we synthesized successfully two chiral half units, $\mathbf{2^{RR}}$ and $\mathbf{2^{SS}}$, by reacting **1** with an excess of enantiomerically pure (*R*,*R*)- or (*S*,*S*)-*trans*-1,2-cyclohexanediamine, respectively, for six days (Scheme 1).[44] Condensation of three equivalents of 3,5-di-*tert*-butylsalicylaldehyde with the half units $\mathbf{2^{RR}}$ and $\mathbf{2^{SS}}$ yielded the corresponding enantiomerically pure chiral ligands H_6chand^{RR} and H_6chand^{SS}, respectively.[44] To synthesize the half unit $\mathbf{2^{rac}}$, the above-stated synthetic protocol has been applied. Specifically, triketone **1** has been reacted with excess racemic *trans*-1,2-cyclohexanediamine for 20 h to yield the half unit $\mathbf{2^{rac}}$ that upon further condensation with three equivalents of 3,5-di-*tert*-butylsalicylaldehyde provides the corresponding racemic ligand H_6chand^{rac}.

The reaction of **1** with racemic *trans*-1,2-cyclohexanediamine (*R*,*R* and *S*,*S* enantiomers) can provide principally four different isomers of half unit **2**: (*R*,*R*)(*R*,*R*)(*R*,*R*), (*S*,*S*)(*S*,*S*)(*S*,*S*), (*R*,*R*)(*R*,*R*)(*S*,*S*), and (*S*,*S*)(*S*,*S*)(*R*,*R*). The first and latter two form enantiomeric pairs that are diastereomeric to each other. It is interesting to note that **1** upon reaction with excess enantiomerically pure (*R*,*R*)- or (*S*,*S*)-*trans*-1,2-cyclohexanediamine for 20 h as in the reaction of $\mathbf{2^{rac}}$ provides a mixture with the intermediate condensation product containing only two acetyl groups converted to ketimine units as the main component. A complete conversion to $\mathbf{2^{RR}}$ and $\mathbf{2^{SS}}$ requires six days. This implies that the third condensation is slower, if only one enantiomer of the diamine is used in comparison to a racemic mixture. A reason for this might be attributed to some steric crowding for the three pendent arms with the same chirality of the diamine backbone. As a direct consequence, the bulk material of the half unit $\mathbf{2^{rac}}$ and the ligand H_6chand^{rac} should not be a statistical mixture of the four possible isomers, but should contain the racemic (*R*,*R*)(*R*,*R*)(*S*,*S*) and (*S*,*S*)(*S*,*S*)(*R*,*R*) configurations as the main products. The NMR spectra of $\mathbf{2^{rac}}$ and H_6chand^{rac} provide a large set of multiplets of higher order. However, the ketimine CH_3 groups in the half unit $\mathbf{2^{rac}}$ give rise to three sharp singlets. By taking into account that the (*R*,*R*)(*R*,*R*)(*R*,*R*)/(*S*,*S*)(*S*,*S*)(*S*,*S*) pair should provide one CH_3 signal and the (*R*,*R*)(*R*,*R*)(*S*,*S*)/(*S*,*S*)(*S*,*S*)(*R*,*R*) pair should provide two CH_3 signals in a 2:1 ratio shows that $\mathbf{2^{rac}}$ is actually a mixture of two diastereomers with (*R*,*R*)(*R*,*R*)-(*S*,*S*)/(*S*,*S*)(*S*,*S*)(*R*,*R*) formed in 85 and (*R*,*R*)(*R*,*R*)(*R*,*R*)/(*S*,*S*)-(*S*,*S*)(*S*,*S*) in 15% yield.

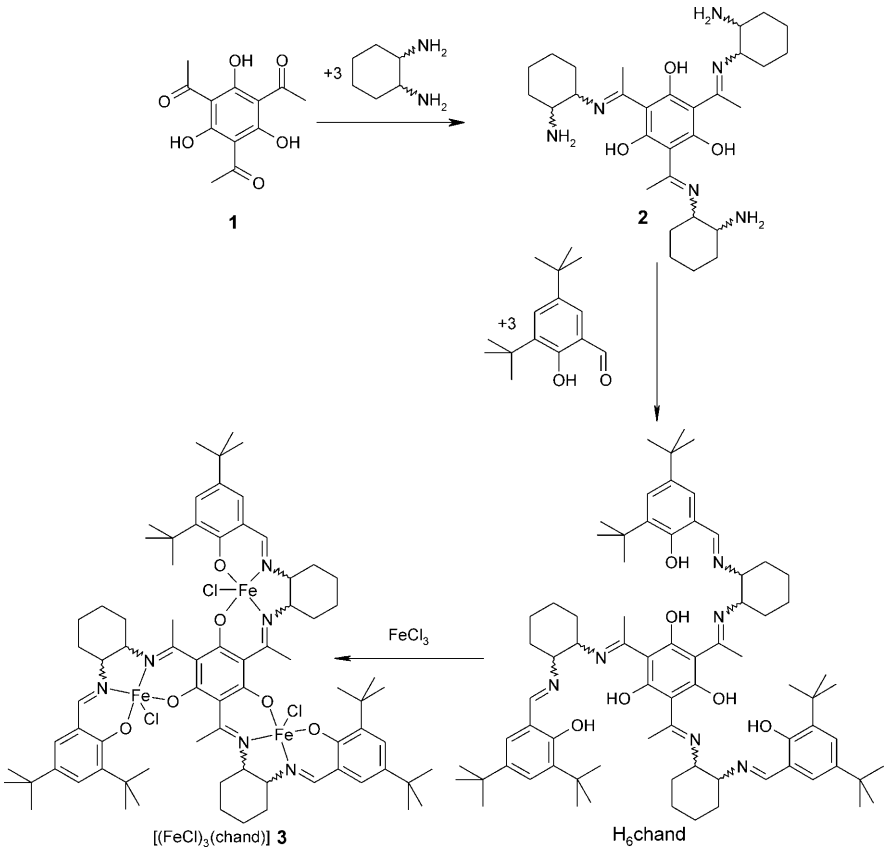

Scheme 1. Synthesis of chiral half units **2** and complexes **3**.

The reaction of one equivalent of the ligand (either H_6chand^{rac} or H_6chand^{RR}) with approximately three equivalents of anhydrous $FeCl_3$ in CH_3CN or in a CH_3CN/MeOH solvent mixture results in the separation of purple microcrystalline trinuclear Fe^{III} triplesalen complexes. Recrystallization of the microcrystalline solid from a CH_2Cl_2/CH_3CN and a CH_2Cl_2/CH_3CN/MeOH solvent mixture provided single crystals of complex $\mathbf{3^{rac}}$ and complex $\mathbf{3^{RR}}$, respectively (vide infra), suited for single-crystal X-ray diffraction.

The IR spectra of $\mathbf{2^{rac}}$ and $\mathbf{2^{RR}}$ are almost identical and provide a sharp band at around 1533 cm^{-1} due to a ν(C=N) vi-

bration of the ketimine units. In the IR spectra of both ligands, H_6chand^{rac} and H_6chand^{RR}, a new band appears at 1628 cm^{-1} due to a ν(C=N) vibration of the aldimine units. The IR spectra of **3^{rac}** and **3^{RR}** exhibit no significant differences. Upon complexation, the ν(C=N) vibration band appearing in the ligand spectrum at 1628 shifts to 1626 cm^{-1}, whereas the band at 1533 shifts to 1537 cm^{-1}. The strong bands at 1479 and at 1254 cm^{-1} are attributed to ν(C=C) vibrations of the aromatic rings and to phenolic ν(C–O) vibrations, respectively.

Mass spectrometry has been found as an important tool to characterize triplesalen half units, ligands, and corresponding iron complexes. The ESI (positive mode) mass spectra of the triplesalen half units and the ligands show $[M+H]^+$ as base peaks (100%). The MALDI-TOF-mass spectrum of complex **3^{rac}** shows peaks at m/z: 1457.0 and 1421.9 that correspond to the composition $[Fe_3Cl_3(chand^{rac})]^+$ and $[Fe_3Cl_2(chand^{rac})]^+$, respectively. The MALDI-TOF-mass spectrum of **3^{RR}** includes a peak at m/z: 1385.9 corresponding to the composition $[Fe_3Cl(chand^{RR})]^+$ together with the peaks at m/z: 1457.1 and 1422.0.

Molecular and crystal structures: The crystal structures of the ligand $H_6chand^{rac}\cdot 2\,CH_3CN\cdot MeOH$ and the complexes $[(FeCl)_3(chand^{rac})]$ (**3^{rac}**) and $[(FeCl)_3(chand^{RR})]$ (**3^{RR}**) were determined by single-crystal X-ray diffraction at 173 K. First, the molecular structures of H_6chand^{rac}, **3^{rac}**, and **3^{RR}** are described followed by a comparative analysis of bond and structural parameters. Finally, the crystal structures of **3^{rac}** and **3^{RR}** are illustrated.

The triplesalen ligand $H_6chand^{rac}\cdot 2\,CH_3CN\cdot MeOH$ crystallizes in the space group $P2_1/n$. The asymmetric unit of the racemic ligand H_6chand^{rac} contains one enantiomer of the molecule with the other enantiomer generated by a crystallographic center of inversion and a mirror plane (the unit cell contains four molecules, two of each enantiomer). The molecular structure of one enantiomer of H_6chand^{rac} is given in Figure 1 (thermal ellipsoid plot in Figure S1, Supporting Information). The configurations of the *trans*-cyclohexanediimine backbone for this enantiomer are 13*R*,18*R*, 23*S*,28*S*, and 33*S*,38*S*. It is interesting to note that the two pendent arms of the same chirality of the cyclohexanediimine parts are to the same side with regard to the central phloroglucinol unit, whereas the third pendent arm of opposite chirality points to the opposite side. This corroborates the argument given in the synthesis and characterization section that the third pendant arm of the same chirality would exhibit steric crowding.

The racemic complex $[(FeCl)_3(chand^{rac})]$ (**3^{rac}**) crystallizes with one molecule in the asymmetric unit in the chiral space group $P6_1$, that is, a spontaneous resolution of the enantiomers upon crystallization has occurred. The chiral complex $[(FeCl)_3(chand^{RR})]$ (**3^{RR}**) crystallizes in the chiral space group $P2_12_12_1$.

The molecular structures of **3^{rac}** and **3^{RR}** are shown in Figure 2a and b, respectively. In both complexes, a six-fold deprotonated triplesalen ligand coordinates three Fe^{III} ions in a typical salen-like square-planar coordination environment. The coordination of one Cl^- ion per Fe^{III} ion results in approximate square-pyramidal coordination environments (τ values:[77] **3^{rac}**: 0.18, 0.38, and 0.20 for Fe1, Fe2, and Fe3, respectively; **3^{RR}**: 0.12, 0.26, and 0.22 for Fe1, Fe2, and Fe3, respectively). In **3^{rac}**, the Fe1, Fe2, and Fe3 atoms are extruded at 0.59, 0.61, and 0.55 Å, respectively, out of the basal coordination plane consisting of the N_2O_2 donor atoms of the ligand $(chand^{rac})^{6-}$ in the direction of the apical chloride. In **3^{RR}**, the Fe1, Fe2, and Fe3 atoms are lying above the best N_2O_2 plane at a respective distance of 0.58, 0.60, and 0.62 Å towards the apical chloride atom.

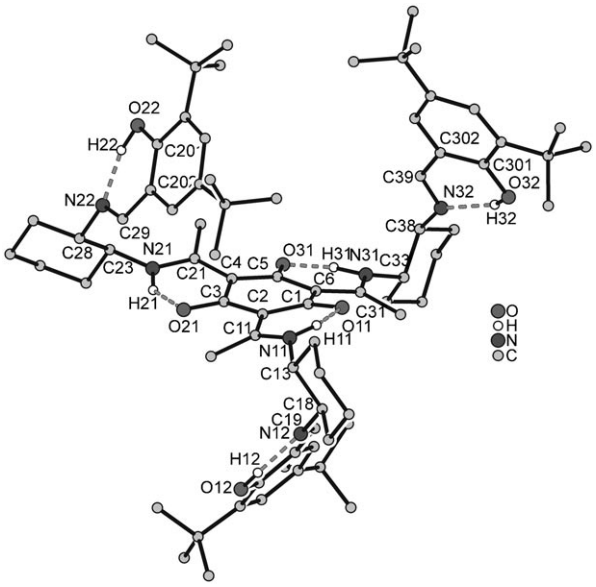

Figure 1. Molecular structure of the ligand H_6chand^{rac} in crystals of $H_6chand^{rac}\cdot 2\,CH_3CN\cdot MeOH$ in a ball and stick presentation. The enantiomer shown has the (13*R*,18*R*)(23*S*,28*S*)(33*S*,38*S*) configuration. Solvent molecules and hydrogen atoms have been omitted for clarity despite N–H and O–H hydrogen atoms.

In complex **3^{RR}**, all the *trans*-cyclohexanediimine backbones are in an *R*,*R* configuration and the chloride ions attached to Fe1, Fe2, and Fe3 atoms are in a *cis* position to each other. It is noticeable that the position of the Fe2 atom is disordered by 10% to the Fe2A atom. In complex **3^{rac}**, the *trans*-cyclohexanediimine moieties exhibit different configurations. In the molecule shown in Figure 2a, the *trans*-13,18-cyclohexanediimine ring with N11 and N12 atoms is in an *R*,*R* configuration, whereas the two other atoms are in the *S*,*S* configuration. This goes along with Cl1 bound to Fe1 (cyclohexadiamine ring in a *R*,*R* configuration), which points in the opposite direction relative to Cl2 bound to Fe2 and Cl3 bound to Fe3 (cyclohexadiamine rings in a *S*,*S* configuration). The absolute orientation of Cl1 in **3^{rac}** corresponds to the orientations of all three chlorides in **3^{RR}** (all cyclohexanediamine rings are in a *R*,*R* configuration). Hence, it is evident that the position of the chloride atom is highly dependent on the configuration of the *trans*-cyclohexanediimine backbone.

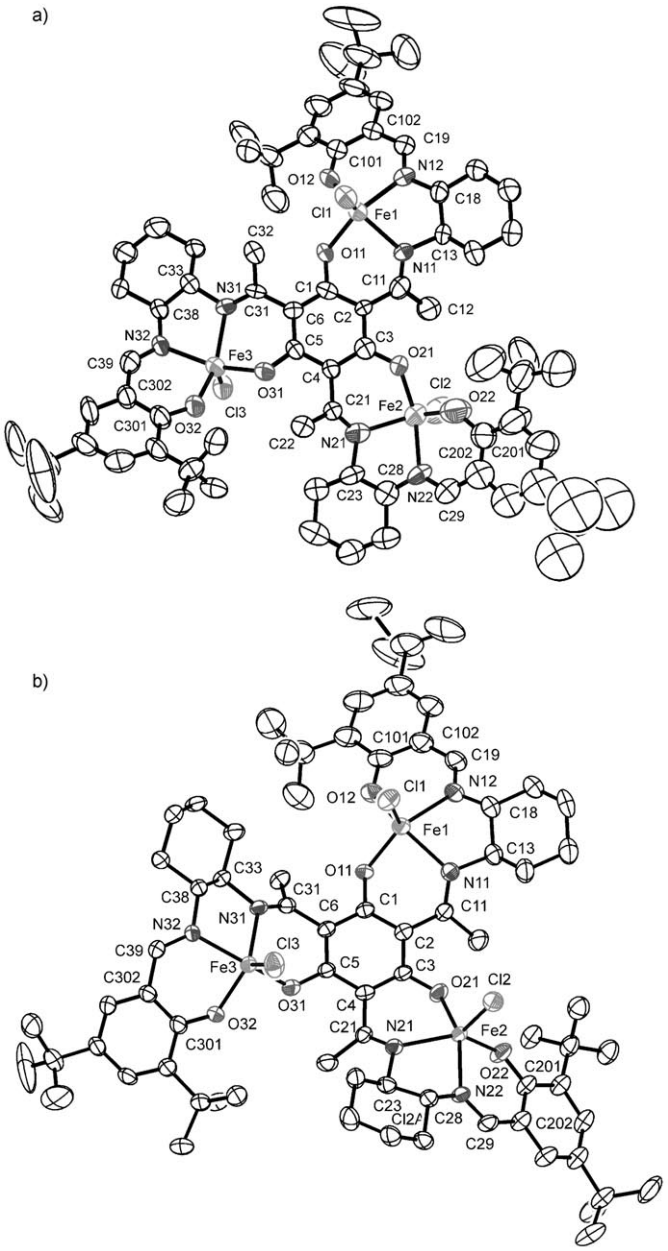

Figure 2. Molecular structures of the trinuclear complexes a) $\mathbf{3^{rac}}$ and b) $\mathbf{3^{RR}}$; thermal ellipsoids are drawn at the 50% probability level; hydrogen atoms are omitted for clarity.

Table 2. Selected interatomic distances [Å] for H_6chand^{rac}, $\mathbf{3^{rac}}$, and $\mathbf{3^{RR}}$.

	H_6chand^{rac}	$\mathbf{3^{rac}}$	$\mathbf{3^{RR}}$
Fe1–O11		1.894(7)	1.878(2)
Fe1–O12		1.876(8)	1.898(2)
Fe2–O21		1.862(7)	1.885(2)
Fe2–O22		1.860(10)	1.881(2)
Fe3–O31		1.880(7)	1.894(2)
Fe3–O32		1.890(8	1.902(2)
Fe1–N11		2.127(9)	2.132(3)
Fe1–N12		2.070(9)	2.076(3)
Fe2–N21		2.113(11)	2.142(3)
Fe2–N22		2.085(10)	2.077(3)
Fe3–N31		2.142(8)	2.169(2)
Fe3–N32		2.046(8)	2.061(2)
Fe1–Cl1		2.205(5)	2.217(1)
Fe2-Cl2		2.215(5)	2.194(2)
Fe3–Cl3		2.212(5)	2.192(1)
C1–O11	1.277(5)	1.344(12)	1.312(4)
C101–O12	1.359(5)	1.337(14)	1.318(4)
C3–O21	1.259(5)	1.322(12)	1.305(4)
C201–O22	1.356(5)	1.358(15)	1.319(4)
C5–O31	1.264(5)	1.307(11)	1.303(4)
C301-O32	1.355(5)	1.322(12)	1.315(4)
C11–N11	1.327(5)	1.308(14)	1.302(4)
C19–N12	1.284(5)	1.324(13)	1.279(5)
C21–N21	1.307(5)	1.250(14)	1.304(4)
C29–N22	1.279(5)	1.266(16)	1.282(4)
C31–N31	1.304(5)	1.273(12)	1.294(4)
C39–N32	1.279(5)	1.278(13)	1.271(4)
C2–C11	1.429(5)	1.475(15)	1.471(4)
C4–C21	1.427(6)	1.472(14)	1.474(4)
C6–C31	1.428(5)	1.465(14)	1.475(4)
C102–C19	1.456(6)	1.443(16)	1.425(6)
C202-C29	1.462(6)	1.381(19)	1.437(5)
C302–C39	1.445(6)	1.426(14)	1.451(5)
Fe1···Fe2		7.391(2)	7.249(1)
Fe2···Fe3		7.177(2)	7.056(1)
Fe1···Fe3		7.371(2)	7.045(1)

Selected interatomic distances are summarized in Table 2. The mean Fe–O^{Ph}, Fe–N, and Fe–Cl bond lengths for $\mathbf{3^{rac}}$ ($\mathbf{3^{RR}}$) are 1.88 (1.89), 2.10 (2.11), and 2.21 (2.20) Å, respectively. These are in good agreement with the other Fe^{III} chloride complexes of salen-type ligands.[78–87] On the other hand, the bond lengths in the ligand show some interesting features. In the molecular structure of the ligand H_6chand^{rac}, the average C–C distance of the central C_6 ring is 1.45 Å, which is longer than the average C–C bond length of the terminal benzene rings (1.40 Å) and considerably closer to the typical values of a C–C single bond length. Furthermore, the central C_6 ring (phloroglucinol unit) is no longer in a planer form but a little bit twisted as evidenced by the largest distance of a constituting carbon atom of 0.10 Å from the best plane. For the terminal benzene rings, the strongest deviation is only 0.02 Å. In the trinuclear complexes, the central C–C bond lengths are shortened to 1.41 and 1.42 Å for $\mathbf{3^{rac}}$ and $\mathbf{3^{RR}}$, respectively, in comparison to H_6chand^{rac}, whereas the terminal benzene rings exhibit a mean C–C bond length of 1.40 Å. Additionally, the deviation of the central benzene ring from planarity is not pronounced in the complexes (largest deviation from the best plane is 0.03 and 0.01 Å for $\mathbf{3^{rac}}$ and $\mathbf{3^{RR}}$, respectively).

The longer C–C bond lengths in the central ring of H_6chand^{rac} coincide with shorter mean C–O lengths (value for terminal rings in parenthesis) of 1.27 (1.36) Å, longer C–N lengths of 1.31 (1.28) Å, and shorter C^{Ar}–C bond lengths of 1.43 (1.45) Å. These bond lengths are a clear indication that in the ligand the central moiety is in the keto–enamine form rather than in the conventionally assumed phenol–imine form.[88,89] This bond-length-based assignment is corroborated by difference Fourier synthesis. The position of the hydrogen atoms in the central moiety have been found to localize on N11, N21, and N31 nitrogen atoms (N11–H11: 0.96, N21–H21: 0.92, N31–H31 1.05 Å), rather than on O11,

O21, and O31 oxygen atoms. Contrarily, at the terminal phenols the hydrogen atoms could be located at the phenol oxygen atoms and not the imine nitrogen atoms. In conjunction with the structural parameters in bond distances it is clearly established that the terminal donor sites in H_6chand^{rac} are in the usual phenol–imine form and not in the tautomeric keto–enamine form.

In the complexes, the acidic hydrogen atoms are absent and the resulting forms, that is, the phenolate–imine and keto–enamide, are no longer tautomers but rather resonance structures of a delocalized system. From a comparison of the relevant bond distances, the prevalence of the usually assumed phenolate–imine resonance structure is indicated. However, a partial loss of the central π system as evidenced by C–C bond lengths of 1.41–1.42 Å is the main result of this structural analysis.

Trinuclear triplesalen complexes are known to exhibit various degrees of ligand folding.[32,35,37–39,42,44] A regular ligand folding results in an overall bowl-shaped molecular structure for the trinuclear Cu^{II} and Ni^{II} complexes of $(talen^{tBu_2})^{6-}$. We have applied several parameters for a quantitative description of the ligand folding in the study of the trinuclear triplesalen complexes.[35,39] It turned out that the best parameters to quantitatively describe the ligand folding are the bent angles $\phi_{central}$ and $\phi_{terminal}$. The bent angle ϕ (introduced by Cavallo and Jacobsen)[90] is defined by $\phi = 180° - <(M\text{-}X_{NO}\text{-}X_R)$ (X_{NO}: midpoint of adjacent N and O donor atoms, X_R: midpoint of the six-membered chelate ring containing the N and O donor atoms). We identified the bent angles $\phi_{central}$ and $\phi_{terminal}$ in trinuclear Cu^{II} and Ni^{II} triplesalen complexes best suited to differentiate between a bending along an idealized line through neighboring N and O ligands and a line perpendicular to the former, resulting in a helical distortion.[35,39] The application to the heptanuclear complexes $[Mn_6Cr]^{3+}$, $[Mn_6Fe]^{3+}$, and $[Mn_6Co]^{3+}$ also showed that a strong folding occurred at the O^{Ph}–N^{imine} vector of the central unit and only a minor folding appeared at the terminal phenolates.[37,42,47] Common to the Cu^{II}, Ni^{II}, and Mn^{III} ions in these complexes is a relatively well-defined planar N_2O_2 plane of the salen-like ligand compartment. This is in contrast to the five-coordinate Fe^{III} ions in **3**^{rac} and **3**^{RR}. The coordination environment exhibits a more or less strong deviation from square-pyramidal to triginal-bipyramidal (τ values vide supra) with the central phenolate and the terminal imine donors as axial ligands.

Applying the usual parameters (Table 3) results in no clear trend in the folding, which is also evident in the two structural presentations provided in Figure 3. While the different cyclohehanediamine configurations in **3**^{rac} prohibit an overall regular folding, the ligand folding in **3**^{RR} does also not provide a bowl-shaped structure observed in the trinuclear complexes of the ligand $(talen^{tBu_2})^{6-}$. This is mainly evident by the relative bendings of the central phenolates and the terminals phenolates, which are in opposite directions in **3**^{RR}, but in the same direction in $(talen^{tBu_2})^{6-}$ complexes.

The chloride atoms Cl2 bound to Fe2 in **3**^{rac} form a weak intermolecular interaction (3.426 Å) to Fe3 of the next tri-

Table 3. Selected structural properties for the iron triplesalen complexes **3**^{rac} and **3**^{RR}.

		3^{rac}	**3**^{RR}
d [Å][a]	Fe1	−0.66	0.84
	Fe2	0.57	0.71
	Fe3	0.93	1.20
α [°][b]	Fe1	12.8	16.8
	Fe2	22.4	22.4
	Fe3	14.2	25.5
β [°][c]	Fe1	39.7	14.4
	Fe2	34.0	18.3
	Fe3	24.7	5.9
γ [°][d]	Fe1	32.2	19.9
	Fe2	13.9	35.0
	Fe3	15.7	23.2
$\phi_{central}$ [°]	Fe1	20.8	22.0
	Fe2	19.9	14.2
	Fe3	18.6	32.9
$\phi_{terminal}$ [°]	Fe1	11.6	14.1
	Fe2	23.2	17.5
	Fe3	12.6	25.0

[a] d is the shortest distances of an Fe^{III} ion from the best plane formed by the six carbon atoms of the central benzene ring of the phloroglucinol unit. A negative value corresponds to a displacement to the other side of the central plane. [b] α is the angle between the best plane of 1) N_2O_2 and 2) the benzene of the phloroglucinol unit. [c] β is the angle between the best plane of 1) N_2O_2 and 2) the terminal phenolate. [d] γ is the angle between the best plane of 1) the benzene of the phloroglucinol unit and 2) the benzene of the terminal phenolate.

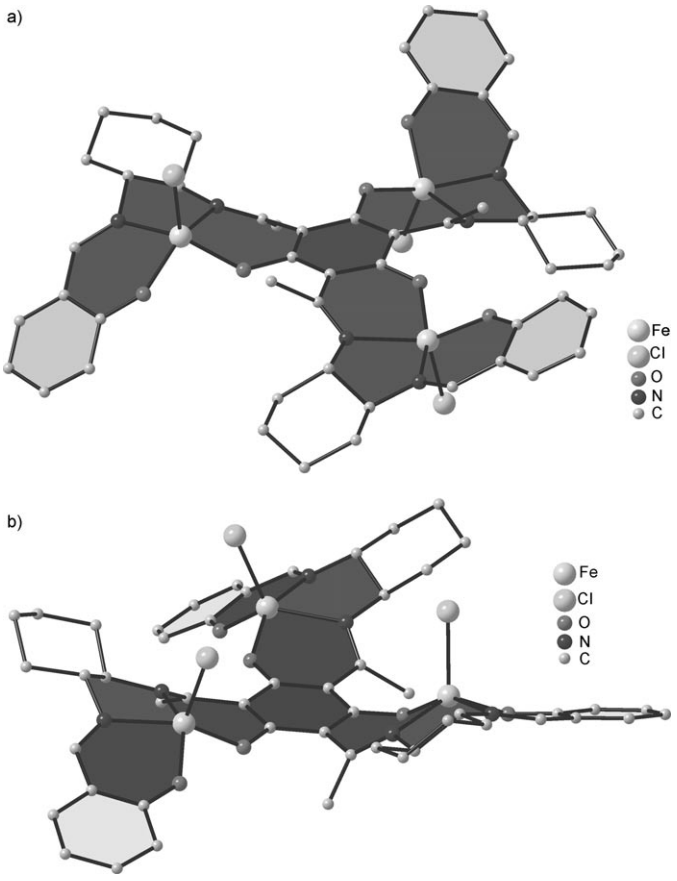

Figure 3. Molecular structures of a) **3**^{rac} and b) **3**^{RR}, which demonstrate the unregular ligand folding. The *tert*-butyl groups were omitted for clarity.

plesalen complex (Figure 4a). This chain formation occurs along a C_3 axis running along *c* leading to a helical structure. These helices pack along *c* resulting in very large chiral

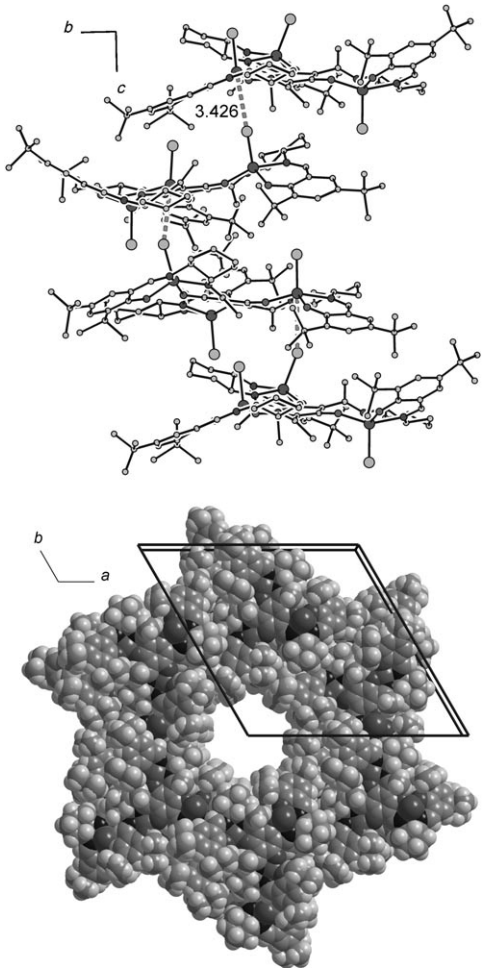

Figure 4. a) Intermolecular Cl···Fe interactions in $\mathbf{3}^{rac}$ leading to helices along *c*. b) Space-filling model of $\mathbf{3}^{rac}$ to visualize the large chiral channels along *c*.

channels (Figure 4b). Though we cannot rule out some ill-defined solvent molecule, no solvent molecule has been found inside the channels. The diameter of these channels is ~14.5 Å based on atom to atom distances and ~11 Å considering van der Waals radii. These empty channels make up 33.6% of the volume of the crystals. In $\mathbf{3}^{RR}$, there are no specific intermolecular interactions. However, large empty voids of 560 Å^3 are apparent.

Mössbauer spectroscopy: Mössbauer spectra of $\mathbf{3}^{rac}$ and $\mathbf{3}^{RR}$ at 80 K are shown in Figure 5. Both spectra exhibit a single unsymmetrical quadrupole doublet with isomer shifts (δ) and quadrupole splittings ($|\Delta E_Q|$) of $\delta = 0.44$ mm s^{-1}, $|\Delta E_Q| = 1.10$ mm s^{-1} for $\mathbf{3}^{rac}$, and $\delta = 0.44$ mm s^{-1}, $|\Delta E_Q| = 1.13$ mm s^{-1} for $\mathbf{3}^{RR}$. These parameters are close to previous-

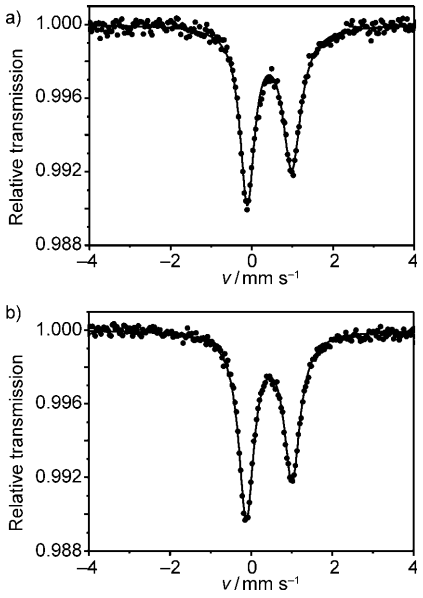

Figure 5. ^{57}Fe Mössbauer spectra of a) $\mathbf{3}^{rac}$ and b) $\mathbf{3}^{RR}$ measured at 80 K. ●: Exp; ——: Sim.

ly reported square-pyramidal FeN_2O_2Cl salen systems[79,91] and contain the ferric high-spin $S_i = 5/2$ configuration for the iron ions.

Electronic absorption spectrum: The electronic absorption spectra (10000–40000 cm^{-1}) of the half units ($\mathbf{2}^{rac}$ and $\mathbf{2}^{RR}$), the free ligands (H_6chand^{rac} and H_6chand^{RR}), and the corresponding complexes ($\mathbf{3}^{rac}$ and $\mathbf{3}^{RR}$) in CH_2Cl_2 are shown in Figure 6, whereas the spectral data are summarized in

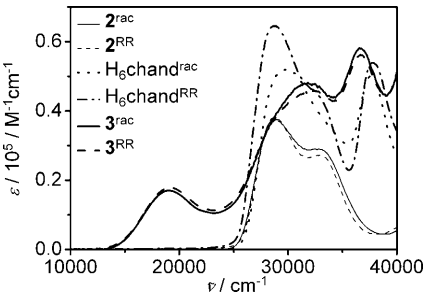

Figure 6. Electronic absorption spectra of $\mathbf{2}^{rac}$, $\mathbf{2}^{RR}$, H_6chand^{rac}, H_6chand^{RR}, $\mathbf{3}^{rac}$, and $\mathbf{3}^{RR}$ measured at ambient temperatures in CH_2Cl_2.

Table 4. It should be noted that the spectra of the diastereomeric pairs, that is, $\mathbf{2}^{rac}$ and $\mathbf{2}^{RR}$, H_6chand^{rac} and H_6chand^{RR}, and $\mathbf{3}^{rac}$ and $\mathbf{3}^{RR}$, are not identical with the strongest differences observed in the spectra of the two ligands.

The spectra of the two triplesalen half units $\mathbf{2}^{rac}$ and $\mathbf{2}^{RR}$ exhibit two strong absorption features at ~29000 and ~33000 cm^{-1}. These transitions have been assigned to π–π* transitions involving the ketimine groups.[35] A strong feature between 35000 and 40000 cm^{-1} for π–π* transitions associated with the phenolic chromophore is not observed in

Table 4. Spectral data of the triplesalen half units, ligands, and trinuclear iron complexes.

	$\tilde{\nu}$ [cm^{-1}] (ε [$M^{-1}cm^{-1}$])
$\mathbf{2}^{rac}$	28950(37400), 33150(28900)
$\mathbf{2}^{RR}$	28600(38000), 33000(27350)
H_6chand^{rac}	29750(51900), 33050^{sh}, 37600(50000)
H_6chand^{RR}	28750(64550), 32500^{sh}, 37800(53900)
$\mathbf{3}^{rac}$	18950(17000), 31900(47900), 36650(57900)
$\mathbf{3}^{RR}$	19250(17850), 32500(45650), 36650(56200)

the half units. Interestingly, by adding the terminal imine–phenol units, that is, on going from $\mathbf{2}^{X}$ to H_6chand^{X}, a strong absorption feature at ~38000 cm^{-1} appears with some intensity modification in the 25000–35000 cm^{-1} region. This implies that the terminal phenol-imine units absorb mainly at higher energies (35000–40000 cm^{-1}), whereas the lower absorptions at 25000–35000 cm^{-1} are mainly due to the central keto–enamine unit, which provides a large delocalized π system. Despite some changes in the region above 25000 cm^{-1}, the two Fe^{III} complexes $\mathbf{3}^{rac}$ and $\mathbf{3}^{RR}$ exhibit a new strong band at ~19000 cm^{-1}. This band is attributed to phenolic oxygen(p_π) to $Fe^{III}(d_{\pi^*})$ charge-transfer transitions.[81,92–94]

Magnetic measurements: Variable-temperature magnetic susceptibility measurements have been measured on powdered samples of $\mathbf{3}^{rac}\cdot1.5H_2O$ and $\mathbf{3}^{RR}$ in the temperature range of 2–290 K with an applied field of 1 T (Figure 7). $\mathbf{3}^{rac}\cdot1.5H_2O$ and $\mathbf{3}^{RR}$ show $\mu_{eff}=10.10$ and 10.46 μ_B at 290 K, respectively. These values are close to the expected μ_{eff} value for three noninteracting high-spin $Fe^{III}(d^5)$ centers ($\mu_{eff}=10.25\ \mu_B$, $g=2.00$). The μ_{eff} value for $\mathbf{3}^{rac}\cdot1.5H_2O$ remains roughly constant up to 40 K. Below 40 K, a pronounced decrease in μ_{eff} occurs resulting in $\mu_{eff}=5.61\ \mu_B$ at 2 K. Complex $\mathbf{3}^{RR}$ shows almost a temperature-independent value of $\mu_{eff}=10.46\ \mu_B$ up to 15 K. Below 15 K, the μ_{eff} value decreases abruptly to $\mu_{eff}=6.81\ \mu_B$ at 2 K. The close resemblance of the μ_{eff} value between the temperature range 40–290 K for $\mathbf{3}^{rac}\cdot1.5H_2O$ and 15–290 K for $\mathbf{3}^{RR}$ indicates that both complexes are almost noninteracting trinuclear high-spin Fe^{III} systems.

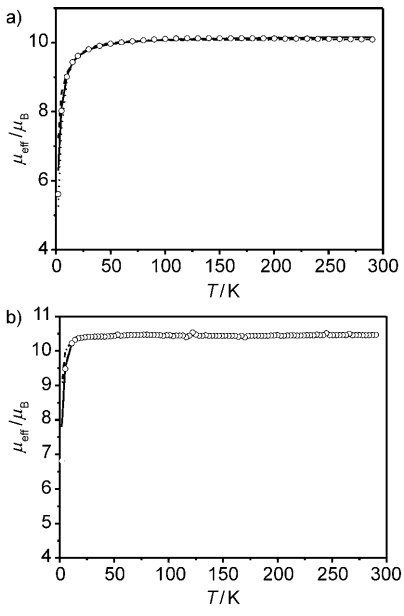

Figure 7. Temperature-dependence of the effective magnetic moment, μ_{eff}, of a) $\mathbf{3}^{rac}\cdot1.5H_2O$ (——: $g=1.99$, $J=-0.14\ cm^{-1}$, $D=0$; -----: $g=1.97$, $J=0$, $D=-8.2\ cm^{-1}$; •••••: $g=1.99$, $J=-0.12\ cm^{-1}$, $D=-2.0\ cm^{-1}$; ○: Exp) and b) $\mathbf{3}^{RR}$ measured at 1 T (——: $g=2.04$, $J=\theta=0$, $D=-2.5\ cm^{-1}$; ——: $g=2.04$, $J=-0.0015\ cm^{-1}$, $D=\theta=0$; •••••: $g=2.04$, $\theta=-0.27$ K, $D=J=0$; -•-•-: $g=2.04$, $J=0.0015\ cm^{-1}$, $D=-2.7\ cm^{-1}$; ○: Exp).

The data were analyzed by full-matrix diagonalization of the appropriate spin-Hamiltonian [Eq. (1)] for trinuclear ferric high-spin complexes including isotropic HDvV exchange, zero-field splitting, and Zeeman interactions.[95]

$$\hat{H} = -2J(S_1S_2 + S_2S_3 + S_3S_1) + \sum_{i=1}^{3}\left(D\left(S_{z,i}^2 - \frac{1}{3}S_i(S_i+1)\right)\right) + \mu_B\sum_{i=1}^{3}(gS_iB) \quad (1)$$

Magnetic moments were obtained from numerically generated derivatives of the eigenvalues of Equation (1) and summed up over 16-field orientations along a 16-point Lebedev grid to account for the powder distribution of the sample.

The decrease of μ_{eff} in the low-temperature range could be either due to saturation effects (which are taken into account in our simulation), a weak *anti*-ferromagnetic intramolecular interaction between the high-spin $Fe^{III}(d^5)$ centers, zero-field splitting, and/or intermolecular antiferromagnetic interactions. Simulations with no zero-field splitting (isotropic limit), with no exchange interaction (uncoupled limit), and by taking into account both contributions were performed. Intermolecular *anti*-ferromagnetic interactions were also considered.

By using the isotropic limit without zero-field splitting, the experimental data are well reproduced by using $g=1.99$, $J=-0.14\ cm^{-1}$ for $\mathbf{3}^{rac}\cdot1.5H_2O$ (—— in Figure 7a) and $g=2.04$, $J=-0.015\ cm^{-1}$ for $\mathbf{3}^{RR}$ (—— in Figure 7b). In the uncoupled limit the experimental results were reproduced by using $g=1.97$, $D=-8.2\ cm^{-1}$ for $\mathbf{3}^{rac}\cdot1.5H_2O$ (—— in Figure 7a) and $g=2.04$, $D=-2.5\ cm^{-1}$ for $\mathbf{3}^{RR}$ (—— in Figure 7b). By considering only intermolecular interactions by using a Curie–Weiss approach, the experimental data for $\mathbf{3}^{RR}$ were fitted with $g=2.04$ and $\theta=-0.27$ K (••••• in Figure 7b). Furthermore, by considering interactions between the Fe^{III} centers and the presence of zero-field splitting in the system, the experimental data could be simulated by using the following parameters: $g=1.99$, $D=-2.0\ cm^{-1}$, $J=-0.12\ cm^{-1}$ for $\mathbf{3}^{rac}\cdot1.5H_2O$ (••••• in Figure 7a) and $g=2.04$, $D=-2.7\ cm^{-1}$, $J=0.005\ cm^{-1}$ for $\mathbf{3}^{RR}$ (-•-•- in Figure 7b). It is evident from the almost superimposed simulations in Figure 7 that the system is highly over parameterized and the identification of one unique parameter set is mathematically not justified. For this reason, we have only applied a coupling scheme for a trinuclear unit of exact C_3 symmetry,

which is a relative good approximation for $\mathbf{3^{RR}}$, but less good for $\mathbf{3^{rac}}$. Reducing the symmetry would even lead to a more pronounced over parameterization.

To focus further on the low-temperature magnetic behavior of $\mathbf{3^{rac}}\cdot 1.5\,H_2O$ and $\mathbf{3^{RR}}$ we have measured variable-temperature variable-field (VTVH) magnetization data (1, 4, and 7 T), which are strongly sensitive to zero-field splitting effects. Fitting of the VTVH magnetization data for $\mathbf{3^{rac}}\cdot 1.5\,H_2O$ (Figure 8a) indicates the existence of both weak

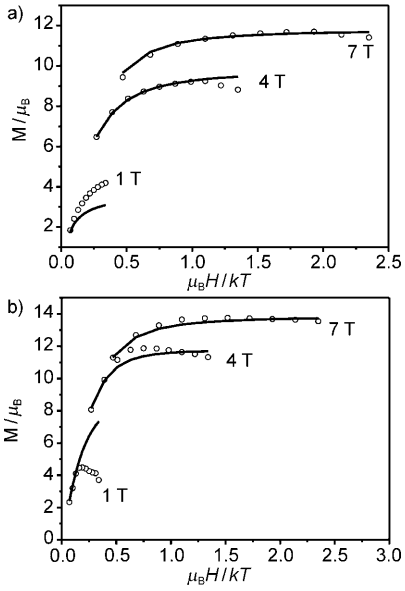

Figure 8. Variable-temperature variable-field (VTVH) magnetization measurements of a) $\mathbf{3^{rac}}\cdot 1.5\,H_2O$ ($g=1.99$, $J=-0.10\ cm^{-1}$, $D=-2.75\ cm^{-1}$; ○: Exp (1 T, 4 T, 7 T)) and b) $\mathbf{3^{RR}}$ at 1 T, 4 T, and 7 T ($g=2.04$, $J=0.005\ cm^{-1}$, $D=-2.0\ cm^{-1}$; ○: Exp (1 T, 4 T, 7 T)).

antiferromagnetic interactions ($J=-0.1\ cm^{-1}$) and zero-field splitting ($D=-2.75\ cm^{-1}$) in the trinuclear high-spin Fe^{III} (d^5, $S_i=5/2$) system. The inspection of VTVH data for $\mathbf{3^{RR}}$ (Figure 8b) shows a decrease in the magnetization value with increasing μ_BH/kT at 4 T, which is more pronounced at 1 T. This decrease is most likely due to dipolar antiferromagnetic intermolecular interactions, which are depressed with increasing magnetic field strength. The experimental magnetization data obtained at 7 T, at which the intermolecular interactions have the weakest effect, can be simulated with $g=2.04$, $D=-2.0\pm0.1\ cm^{-1}$, $J=0.005\pm0.005\ cm^{-1}$.

In summary, the magnetic measurements reveal that in both complexes the intramolecular interactions are only very weak but the Fe^{III} ions possess relatively strong magnetic anisotropies.

Catalytic reactivity: Oxidation of prochiral sulfides to the corresponding sulfoxides: Complex $\mathbf{3^{rac}}$ and $\mathbf{3^{RR}}$ were used as catalysts (5 mol%) to oxidize prochiral sulfides at room temperature under the conditions stated in the Experimental Section. The results are summarized in Tables 4 and 5, respectively. The yields of the sulfoxides as well as the selectivities (sulfoxide to sulfone) are good when using both $\mathbf{3^{rac}}$ and $\mathbf{3^{RR}}$ complexes as the catalyst. The yield appears to depend on the equivalents of the external oxidant PhIO (Table 5). By using NaOCl as an external oxidant, the catalytic oxidation reaction can also be performed. In this case, the selectivity depends on the concentration of NaOCl. When the concentration of NaOCl is in a 10-fold excess to the concentration of thioanisole (Table 3), the selectivity is only 37%. Upon lowering the equivalents of NaOCl to a 2-fold excess relative to the equivalents of thioanisole, 94% selective formation of sulfoxide over sulfone is obtained with 91% conversion of the substrate.

Table 5. Catalytic oxidation of sulfides by using $\mathbf{3^{rac}}$.[a]

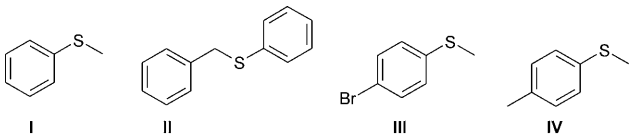

I II III IV

Sulfide	Sulfoxide [%]	Sulfone [%]	Selectivity [%][b]	PhIO (a), NaOCl (b)[c]
I	59	<1	>99	1.1 (a)
I	72	<1	>99	1.5 (a)
I	97	<1	>99	2.2 (a)
I	37	63	37	10 (b)
I	58	42	58	4 (b)
I	86	5	94	2 (b)
II	30	n.d.[d]	100	1.1 (a)
II	84	8	91	2.2 (a)
III	50	2	96	1.1 (a)
III	90	3	97	2.2 (a)
IV	72	1	99	1.1 (a)
IV	98	2	98	2.2 (a)

[a] 5 mol% catalyst, CH_2Cl_2 as the solvent, room temperature. [b] Selectivity = [RSOR′]/[(RSOR′+RSO_2R')]. [c] Values of PhIO (a) and NaOCl (b) correspond to the equivalents of the oxidant to the substrate. [d] n.d. = not detected.

We measured the enantiomeric excess (*ee*) for those catalytic reactions for which the enantiomerically pure chiral complex $\mathbf{3^{RR}}$ was used as the catalyst. The results are listed in Table 6. Though, the enantiomeric excess is low for all the substrates, it is worth noting that on addition of a bulky Br group at the *para* position of the phenyl ring of thioanisole (substrate III), the *ee* increases from 13 to 26%. Similarly, on addition of a bulky phenyl group to the methylene position of the thioanisole (substrate II), 20% *ee* has been

Table 6. Catalytic enantioselective oxidation of sulfides by using $\mathbf{3^{RR}}$.[a]

Sulfide	Sulfoxide [%]	Sulfone [%]	Selectivity [%][b]	*ee* [%] (configuration)[c]
I	95	3	97	13 (*R*)
II	96	4	96	20 (*R*)
II[d]	70	1	98	30 (*R*)
III	84	2	98	26 (*R*)
IV	97	3	97	10 (*R*)

[a] 5 mol% catalyst, 2.2 equivalents of PhIO, CH_2Cl_2 as the solvent, room temperature (unless otherwise stated). [b] Selectivity = [RSOR′]/[(RSOR′+RSO_2R')]. [c] *ee* values were measured by using a chiral OD-H column. [d] 0 °C, 17 h.

achieved. When the catalysis with substrate II is performed at 0 °C, the *ee* value increases from 20 to 30 %, but the yield decreases from 96 to 70 %. Interestingly, for all catalytic reactions using **3^{RR}** as the catalyst production of the *R* over *S* isomer dominates.

Due to a different solubility, we could not adapt the exact catalytic protocol used for the application of [FeCl(salen′)].[96] To have an exact comparability of the catalytic properties of the trinuclear complex **3^{RR}** to its mononuclear analogue, we performed parallel reactions with both catalysts (Table 7) for the asymmetric sulfoxidation of benzyl phenyl sulfide. By using 5 mol % catalyst, the trinuclear complex **3^{RR}** has a better performance with respect to yield and selectivity, whereas the *ee* is tremendously reduced. Going to only 1 mol % reduces the yield for **3^{RR}** from 96 to 9 %. This implies that the reaction of **3^{RR}** is slower than that of [FeCl(salen′)]. Reducing the equivalents of the oxidant from 2.2 to 1.1 decreases the yield for both catalysts but **3^{RR}** has almost a perfect selectivity for the sulfoxide.

Table 7. Catalytic oxidation of benzyl phenyl sulfide by using [$(FeCl)_3$(chand^{RR})] (**3^{RR}**) and [FeCl(salen′)] complexes.[a]

Catalyst ([mol %])	PhIO [equiv]	Sulfoxide [%]	Sulfone [%]	Selectivity [%][b]	*ee* [%] (configuration)[c]
[$(FeCl)_3$(chand^{RR})] (5)	2.2	96	4	96	20 (R)
[FeCl(salen′)] (5)	2.2	78	22	78	63 (R)
[$(FeCl)_3$(chand^{RR})] (1)[d]	2.2	9	n.d.[e]	100	n.m. [e]
[FeCl(salen′)] (1)[d]	2.2	60	2	97	48 (R)
[$(FeCl)_3$(chand^{RR})] (5)	1.1	71	n.d.[e]	100	10 (R)
[FeCl(salen′)] (5)	1.1	82	3	96	47 (R)

[a] All the reactions were carried out for 15 h, CH_2Cl_2 as the solvent, room temperature (unless otherwise stated). Values of PhIO correspond to the equivalent of PhIO to the concentration of the substrate. [b] Selectivity = [RSOR′]/([RSOR′] + [RSO_2R′]). [c] *ee* values were obtained by measuring chiral HPLC by using a chiral OD-H column. [d] Reactions were carried out for 1 h. [e] n.d. = not detected; n.m. = not measured.

These results may be rationalized by the assumption, that the high-valent, catalytically active Fe–O species is stabilized in the trinuclear complex relative to the mononuclear complex. This would explain not only the slower reaction of **3^{RR}** but also its higher selectivity, so that the oxidized species is less capable of oxygenating the sulfoxide product to sulfone.

The assumption of a stabilization of the active Fe–O species in the trinuclear complex is supported by our studies on the trinuclear Ni^{II}_3 and Cu^{II}_3 triplesalen complexes.[35,39] These complexes are either ligand-centered oxidized at the central unit[97] in the case of Cu^{II}_3 or exhibit a valence-tautomerism between a ligand-centered oxidized form and a metal-oxidized Ni^{III} species in the case of Ni^{II}_3. Either form is inherently mixed-valent. A comparison of the potential for oxidation with those of the respective mononuclear analogues provided a stabilization of the oxidized species in the trinuclear complexes relative to the mononuclear salen species. In this respect, the stabilization of the oxidized species leading to a reduced activity and thus a higher selectivity is a cooperative effect in the trinuclear catalysts **3^{RR}** and **3^{rac}**.

The lower *ee* values for the trinuclear catalyst **3^{RR}** than that of the mononuclear reference [FeCl(salen′)] is related to the ligand folding observed for **3^{RR}** (Figure 3), which does not produce a bowl-shaped structure. The structure of [FeCl(salen′)] has not been published yet. However, closely related complexes[84,86,98–100] exhibit only minor ligand foldings. As is evident from Figure 3, the bending of the terminal phenolates is to the opposite direction of the Fe–Cl unit. Assuming a similar orientation in the active high-valent Fe–O species, there is no strong steric hindrance for the attack of a sulfide to the Fe–O unit. Furthermore, the accessibility of the active Fe–O unit must be easier in the trinuclear catalyst relative to the mononuclear analogue. While this result is quite surprising, there are several possibilities in the triplesalen ligand system to increase steric bulk.

Conclusion

Triplesalen ligands bridge three salen coordination environments in a *meta*-phenylene arrangement by a common phloroglucinol backbone. The hexa-anionic forms are triple(tetradentate) ligands and are capable of coordinating three transition-metal ions. The three metal salen subunits are electronically interacting through a strongly conjugated central phloroglucinol unit, which we thought would be useful for cooperative effects in catalysis.[35]

In this respect, we envisioned to incorporate the chiral *trans*-1,2-cyclohexanediamine for the realization of the chiral triplesalen ligand H_6chand as the C_3 symmetric trinucleating extension of Jacobsen's ligand H_2salen′. Herein, we have presented the synthesis and characterization of the two diastereomeric ligands H_6chand^{rac} and H_6chand^{RR} in two steps with the half units **2^{rac}** and **2^{RR}** as intermediates. The former is synthesized from the racemic (*R*,*R*)/(*S*,*S*)-*trans*-1,2-cyclohexanediamine mixture resulting in four stereoisomers. The racemic (*R*,*R*)(*R*,*R*)(*S*,*S*)/(*S*,*S*)(*S*,*S*)(*R*,*R*) pair is obtained in excess to the racemic (*R*,*R*)(*R*,*R*)(*R*,*R*)/(*S*,*S*)(*S*,*S*)(*S*,*S*) pair due to steric hindrance for the formation of the third pendant arm of the same chirality, which are all on the same side relative to the phloroglucinol backbone. The use of the enantiomerically pure (*R*,*R*)-*trans*-1,2-cyclohexanediamine results in the formation of the enantiomerically pure half unit **2^{RR}** corresponding to the (*R*,*R*)(*R*,*R*)(*R*,*R*) isomer. Reaction of the half units with 3,5-di-*tert*-butylsalicylaldehyde provides the racemic ligand H_6chand^{rac} and the enantiomerically pure ligand H_6chand^{RR}. Reaction of the ligands with $FeCl_3$ provided the trinuclear complexes [$(Fe^{III}Cl)_3$(chand^{rac})] (**3^{rac}**) and [$(Fe^{III}Cl)_3$(chand^{RR})] (**3^{RR}**).

The molecular structure of H_6chand^{rac} shows the presence of different tautomers: whereas the terminal phenols are in the conventionally anticipated phenol–imine form, the central unit is in the tautomeric keto–enamine form. Comparison of the structural parameters of the ligand and the com-

plexes reveals that the terminal donors are well described by the phenolate–imine resonance structure, whereas the central donors have also some contributions from the keto–enamide resonance structure. We are currently performing detailed NMR spectroscopic studies on our phloroglucinol-based ligand systems to obtain an experimental handle on the weight of this resonance structure. The presence of this resonance structure might be a reason for the relatively weak ferromagnetic interactions by means of the spin-polarization mechanism through the triplesalen-based systems. This would provide us with a synthetic handle to rationally optimize the strength of the ferromagnetic coupling.

The magnetic measurements reveal quite strong magnetic anisotropies for the high-spin Fe^{III} ions. As the high-spin Fe^{III} ion is usually inherently magnetically isotropic, there have been reports on even stronger anisotropies for salen Fe^{III} complexes in the literature quantified by zero-field splitting parameters $|D|$ of 4–6 cm^{-1},[101] 7.5,[102] 10.2,[103] and 7.2[103] In this respect, the strategy to incorporate salen-like ligand environments to introduce a strong magnetic anisotropy[32,37] seem to work.

Both complexes $\mathbf{3^{rac}}$ and $\mathbf{3^{RR}}$ show good catalytic performance in the sulfoxidation of sulfides relative to mononuclear iron chloride salen systems. They provide high yields and high selectivities favoring the formation of the sulfoxides relative to the corresponding sulfones. However, the chiral catalyst $\mathbf{3^{RR}}$ is not as good in the enantioselective sulfoxidation of prochiral sulfides providing lower *ee* values relative to [FeCl(salen′)]. This might be related to strong ligand foldings observed in $\mathbf{3^{RR}}$, which open up access to the catalytically active Fe–O species.

The high yields and selectivities on the other hand are related to a stabilization of the active high-valent Fe–O species, which results in a slower reaction with less side reactions and more selectivity due to the decreased driving force for overoxidation. The stabilization of the intrinsically mixed valence system occurs by a delocalization over the whole central unit, which involves also some communication with the other two iron centers. In this respect, the trinuclear system exhibits a cooperative effect relative to the mononuclear system by reducing the reactivity of the active species, which is not possible in the mononuclear system.

Acknowledgements

This work was supported by the DFG (FOR945 "Nanomagnets: from Synthesis via Interactions with Surfaces to Function"), the Fonds der Chemischen Industrie, and Bielefeld University. Mr. B. Sammet and Prof. Dr. N. Sewald (Chemistry Department, Bielefeld University) are thankfully acknowledged for assistance in the chiral HPLC measurements.

[1] I. Fernández, N. Khiar, *Chem. Rev.* **2003**, *103*, 3651–3705.
[2] P. Renaud, M. Gerster, *Angew. Chem.* **1998**, *110*, 2704–2722; *Angew. Chem. Int. Ed.* **1998**, *37*, 2562–2579.
[3] H. Pellissier, *Tetrahedron* **2006**, *62*, 5559–5601.
[4] A. Korte, J. Legros, C. Bolm, *Synlett* **2004**, 2397–2399.
[5] M. C. Carreno, G.-H. Torres, M. Ribagorda, A. Urbano, *Chem. Commun.* **2009**, 6129–6144.
[6] K. K. Andersen, *Tetrahedron Lett.* **1962**, *3*, 93–95.
[7] H. B. Kagan, Ed.: I. Ojima, *Asymmetric Synthesis*, VCH, Weinheim, **1993**, pp. 203–226.
[8] S. Colonna, N. Gaggero, L. Casella, G. Carrea, P. Pasta, *Tetrahedron: Asymmetry* **1992**, *3*, 95–106.
[9] J.-M. Brunel, H. B. Kagan, *Bull. Soc. Chim. Fr.* **1996**, *133*, 1109–1115.
[10] S. Colonna, A. Manfredi, M. Spadoni, L. Casella, M. Gullotti, *J. Chem. Soc. Perkin Trans. 1* **1987**, 71–73.
[11] F. Di Furia, G. Licini, G. Modena, R. Motterle, *J. Org. Chem.* **1996**, *61*, 5175–5177.
[12] H. B. Kagan, T. Luukas, M. Eds.: M. Beller, C. Bolm, *Transition Metals for Organic Synthesis*, Wiley-VCH, Weinheim, **1998**, pp. 361–373.
[13] C. Bolm, K. Muniz, J. Hildebrand, *Comprehensive Asymmetric Catalysis*, Springer, Berlin, **1999**, pp. 697–713.
[14] J. Sun, C. Zhu, Z. Dai, M. Yang, Y. Pan, H. Hu, *J. Org. Chem.* **2004**, *69*, 8500–8503.
[15] A. H. Vetter, A. Berkessel, *Tetrahedron Lett.* **1998**, *39*, 1741–1744.
[16] C. Bolm, *Coord. Chem. Rev.* **2003**, *237*, 245–256.
[17] H. Fu, H. Kondo, Y. Ichikawa, G. C. Look, C. H. Wong, *J. Org. Chem.* **2002**, *67*, 7265–7270.
[18] J. K. Whitesell, M. S. Wong, *J. Org. Chem.* **1994**, *59*, 597–601.
[19] K. Nakajima, M. Kojima, K. Toriumi, K. Saito, J. Fujita, *Bull. Chem. Soc. Jpn.* **1989**, *62-62*, 760–767.
[20] J. Burnel, M.-H. B. Kagan, *Bull. Chem. Soc. Fr.* **1996**, *133*, 1109–1115.
[21] C. Sasaki, K. Nakajima, M. Kojima, J. Fujita, *Bull. Chem. Soc. Jpn.* **1991**, *64*, 1318–1324.
[22] C. Bolm, O. A. G. Dabard, *Synlett* **1999**, 360–362.
[23] G. Liu, D. A. Cogan, J. A. Ellman, *J. Am. Chem. Soc.* **1997**, *119*, 9913.
[24] C. Bolm, F. Bienewald, *Angew. Chem.* **1995**, *107*, 2883–2885; *Angew. Chem. Int. Ed. Engl.* **1995**, *34*, 2640–2642.
[25] M. Palucki, P. Hanson, E. N. Jacobsen, *Tetrahedron Lett.* **1992**, *33*, 7111–7114.
[26] K. Noda, N. Hosoya, R. Irie, Y. Yamashita, T. Katsuki, *Tetrahedron* **1994**, *50*, 9609–9618.
[27] J. Legros, C. Bolm, *Angew. Chem.* **2003**, *115*, 5645–5647; *Angew. Chem. Int. Ed.* **2003**, *42*, 5487–5489.
[28] V. K. Sivasubramanian, M. Ganesan, S. Rajagopal, R. Ramaraj, *J. Org. Chem.* **2002**, *67*, 1506–1514.
[29] W. Zhang, E. N. Jacobsen, *J. Org. Chem.* **1991**, *56*, 2296–2298.
[30] K. P. Bryliakov, E. P. Talsi, *Angew. Chem.* **2004**, *116*, 5340–5342.
[31] T. Glaser, M. Gerenkamp, R. Fröhlich, *Angew. Chem.* **2002**, *114*, 3984–3986; *Angew. Chem. Int. Ed.* **2002**, *41*, 3823–3825.
[32] T. Glaser, M. Heidemeier, T. Lügger, *Dalton Trans.* **2003**, 2381–2383.
[33] T. Glaser, T. Lügger, R. Fröhlich, *Eur. J. Inorg. Chem.* **2004**, 394–400.
[34] T. Glaser, M. Heidemeier, S. Grimme, E. Bill, *Inorg. Chem.* **2004**, *43*, 5192–5194.
[35] T. Glaser, M. Heidemeier, R. Fröhlich, P. Hildebrandt, E. Bothe, E. Bill, *Inorg. Chem.* **2005**, *44*, 5467–5482.
[36] T. Glaser, M. Heidemeier, E. Krickemeyer, H. Bögge, *Z. Naturforsch.* **2006**, *61*, 753–757.
[37] T. Glaser, M. Heidemeier, T. Weyhermüller, R.-D. Hoffmann, H. Rupp, P. Müller, *Angew. Chem.* **2006**, *118*, 6179–6183; *Angew. Chem. Int. Ed.* **2006**, *45*, 6033–6037.
[38] T. Glaser, M. Heidemeier, R. Fröhlich, *C. R. Chim.* **2007**, *10*, 71–78.
[39] T. Glaser, M. Heidemeier, J. B. H. Strautmann, H. Bögge, A. Stammler, E. Krickemeyer, R. Huenerbein, S. Grimme, E. Bothe, E. Bill, *Chem. Eur. J.* **2007**, *13*, 9191–9206.
[40] H. Theil, C.-G. Freiherr von Richthofen, A. Stammler, H. Bögge, T. Glaser, *Inorg. Chim. Acta* **2008**, *361*, 916–924.

[41] T. Glaser, H. Theil, M. Heidemeier, *C. R. Chim.* **2008**, *11*, 1121–1136.
[42] T. Glaser, M. Heidemeier, E. Krickemeyer, H. Bögge, A. Stammler, R. Fröhlich, E. Bill, J. Schnack, *Inorg. Chem.* **2009**, *48*, 607–620.
[43] C.-G. Freiherr von Richthofen, C.-G. A. Stammler, H. Bögge, M. W. DeGroot, J. R. Long, T. Glaser, *Inorg. Chem.* **2009**, *48*, 10165–10176.
[44] C. Mukherjee, A. Stammler, H. Bögge, T. Glaser, *Inorg. Chem.* **2009**, *48*, 9476–9484.
[45] H. Theil, R. Fröhlich, T. Glaser, *Z. Naturforsch. B* **2009**, *64*, 1633–1638.
[46] T. Glaser, M. Heidemeier, H. Theil, A. Stammler, H. Bögge, J. Schnack, *Dalton Trans.* **2010**, *39*, 192–199.
[47] E. Krickemeyer, V. Höke, A. Stammler, H. Bögge, J. Schnack, T. Glaser, *Z. Naturforsch. B* **2010**, *65*, 295–303.
[48] H. C. Longuet-Higgins, *J. Chem. Phys.* **1950**, *18*, 265–274.
[49] H. Iwamura, *Adv. Phys. Org. Chem.* **1991**, *26*, 179–253.
[50] K. Yoshizawa, R. Hoffmann, *J. Am. Chem. Soc.* **1995**, *117*, 6921–6926.
[51] D. A. Dougherty, *Acc. Chem. Res.* **1991**, *24*, 88–94.
[52] A. A. Ovchinnikov, *Theor. Chim. Acta* **1978**, *47*, 297–304.
[53] S.-i. Mitsubori, T. Ishida, T. Nogami, H. Iwamura, *Chem. Lett.* **1994**, 285–288.
[54] T. Ishida, S.-i. Mitsubori, T. Nogami, N. Takeda, M. Ishikawa, H. Iwamura, *Inorg. Chem.* **2001**, *40*, 7059–7064.
[55] F. Lloret, G. De Munno, M. Julve, J. Cano, R. Ruiz, A. Caneschi, *Angew. Chem.* **1998**, *110*, 143–145; *Angew. Chem. Int. Ed.* **1998**, *37*, 135–138.
[56] L. C. Francesconi, D. R. Corbin, D. N. Hendrickson, G. D. Stucky, *Inorg. Chem.* **1979**, *18*, 3074–3080.
[57] H. Oshio, *Chem. Commun.* **1991**, 240–241.
[58] J. A. McCleverty, M. D. Ward, *Acc. Chem. Res.* **1998**, *31*, 842–851.
[59] A. M. W. Cargill Thompson, D. Gatteschi, J. A. McCleverty, J. A. Navas, E. Rentschler, M. D. Ward, *Inorg. Chem.* **1996**, *35*, 2701–2703.
[60] V. A. Ung, A. Thompson, D. A. Bardwell, D. Gatteschi, J. C. Jeffery, J. A. McCleverty, F. Totti, M. D. Ward, *Inorg. Chem.* **1997**, *36*, 3447–3454.
[61] I. Fernández, R. Ruiz, J. Faus, M. Julve, F. Lloret, J. Cano, X. Ottenwaelder, Y. Journaux, C. Munoz, *Angew. Chem.* **2001**, *113*, 3129–3132; *Angew. Chem. Int. Ed.* **2001**, *40*, 3039–3042.
[62] X. Ottenwaelder, J. Cano, Y. Journaux, E. Riviere, C. Brennan, M. Nierlich, R. Ruiz-Garcia, *Angew. Chem.* **2004**, *116*, 868–870; *Angew. Chem. Int. Ed.* **2004**, *43*, 850–852.
[63] K. B. Hansen, J. L. Leighton, E. N. Jacobsen, *J. Am. Chem. Soc.* **1996**, *118*, 10924–10925.
[64] D. J. Darensbourg, J. C. Yarbrough, *J. Am. Chem. Soc.* **2002**, *124*, 6335–6342.
[65] D. J. Darensbourg, R. M. Mackiewicz, A. L. Phelps, D. R. Billodeaux, *Acc. Chem. Res.* **2004**, *37*, 836–844.
[66] E. N. Jacobsen, *Acc. Chem. Res.* **2000**, *33*, 421–431.
[67] H. Friese, *Chem. Ber.* **1931**, *64*, 2109–2112.
[68] J. F. Larrow, E. N. Jacobsen, Y. Gao, Y. Hong, X. Nie, C. M. Zepp, *J. Org. Chem.* **1994**, *59*, 1939–1942.
[69] SADBS, G. M. Sheldrick, University of Göttingen, Göttingen, **2003**.
[70] G. M. Sheldrick, *Acta Crystallogr. Sect. A* **2008**, *64*, 112–122.
[71] PLATON/SQUEEZE, A. L. Spek, Bijvoet Center for Biomolecular Research, Utrecht University, Utrecht.
[72] R. Hernández-Molina, A. Mederos in *Comprehensive Coordination Chemistry II, Vol. 1* (Eds.: J. A. McCleverty, T. J. Meyer), Elsevier, Oxford, **2004**, pp. 411–446.
[73] A. W. Kleij, *Eur. J. Inorg. Chem.* **2009**, 193–205.
[74] J. Lopez, S. Liang, X. R. Bu, *Tetrahedron Lett.* **1998**, *39*, 4199–4202.
[75] K. B. M. Janssen, I. Laquierra, W. Dehaen, R. F. Parton, I. F. J. Vankelecom, P. A. Jacobs, *Tetrahedron: Asymmetry* **1997**, *8*, 3481–3487.
[76] J.-P. Costes, F. Dahan, A. Dupuis, J.-P. Laurant, *Dalton Trans.* **1998**, 1307–1314.
[77] A. W. Addison, T. N. Rao, J. Reedijk, J. van Rijn, G. C. Verschoor, *Dalton Trans.* **1984**, 1349–1356.
[78] J. E. Davies, B. M. Gatehouse, *Chem. Commun.* **1970**, 1166.
[79] H.-L. Shyu, H.-H. Wei, G.-H. Lee, Y. Wang, *Dalton Trans.* **2000**, 915–918.
[80] M. Gerloch, F. E. Mabbs, *J. Chem. Soc. A* **1967**, 1900–1908.
[81] M. Lubben, A. Meetsma, F. v. Bolhuis, B. L. Feringa, *Inorg. Chim. Acta* **1994**, *215*, 123–129.
[82] H. Fujii, Y. Funahashi, *Angew. Chem.* **2002**, *114*, 3790–3793; *Angew. Chem. Int. Ed.* **2002**, *41*, 3638–3641.
[83] M. Gerloch, F. E. Mabbs, *J. Chem. Soc. A* **1967**, 1598–1608.
[84] Z. Chu, W. Huang, L. Wang, S. Gou, *Polyhedron* **2008**, *27*, 1079–1092.
[85] K. Oyaizu, E. Tsuchida, *Inorg. Chim. Acta* **2003**, *355*, 414–419.
[86] T. Kurahashi, K. Oda, M. Sugimoto, T. Ogura, H. Fujii, *Inorg. Chem.* **2006**, *45*, 7709–7721.
[87] M. Tomita, N. Matsumoto, H. Akagi, H. Okawa, S. Kida, *Dalton Trans.* **1989**, 179–184.
[88] M. Sauer, C. Yeung, J. H. Chong, B. O. Patrick, M. J. MacLachlan, *J. Org. Chem.* **2006**, *71*, 775–788.
[89] J. H. Chong, M. Sauer, B. O. Patrick, M. J. MacLachlan, *Org. Lett.* **2003**, *5*, 3823–3826.
[90] L. Cavallo, H. Jacobsen, *Eur. J. Inorg. Chem.* **2003**, 892–902.
[91] K. J. Berry, P. E. Clark, K. S. Murray, C. L. Raston, A. H. White, *Inorg. Chem.* **1983**, *22*, 3928–3934.
[92] B. P. Gaber, V. Miskowski, T. G. Spiro, *J. Am. Chem. Soc.* **1974**, *96*, 6868–6873.
[93] J. B. H. Strautmann, S. DeBeer George, E. Bothe, E. Bill, T. Weyhermüller, A. Stammler, H. Bögge, T. Glaser, *Inorg. Chem.* **2008**, *47*, 6804–6824.
[94] C. Flassbeck, K. Wieghardt, *Z. Anorg. Allg. Chem.* **1992**, *608*, 60–68.
[95] The program package JulX was used for spin-Hamiltonian simulations and fittings of the data by a full-matrix diagonalization approach (E. Bill, unpublished results).
[96] K. P. Bryliakov, E. P. Talsi, *Chem. Eur. J.* **2007**, *13*, 8045–8050.
[97] S. Walleck, H. Theil, M. Heidemeier, H. Heinze-Brüchner, A. Stammler, H. Bögge, T. Glaser, unpublished results.
[98] H. Fujii, Y. Funahashi, *Angew. Chem.* **2002**, *114*, 3790–3793; *Angew. Chem. Int. Ed.* **2002**, *41*, 3638–3641.
[99] M. Lubben, A. Meetsma, F. von Bolhuis, B. L. Feringa, R. Hage, *Inorg. Chim. Acta* **1994**, *215*, 123–129.
[100] A. V. Wiznycia, J. Desper, C. J. Levy, *Can. J. Chem.* **2009**, *87*, 224–231.
[101] B. J. Kennedy, G. Brain, E. Horn, K. S. Murray, M. R. Snow, *Inorg. Chem.* **1985**, *24*, 1647–1653.
[102] B. J. Kennedy, K. S. Murray, M. R. Snow, *Inorg. Chim. Acta* **1987**, *132*, 153–155.
[103] H.-L. Shyu, H.-H. Wei, G.-H. Lee, Y. Wang, *J. Chem. Soc. Dalton Trans.* **2000**, 915–918.
[104] H. D. Flack, *Acta Cryst.* **1983**, *A39*, 876–881.

Received: April 12, 2010
Published online: July 14, 2010

